GEBZE TECHNICAL UNIVERSITY

Acta Materialia Turcica

Volume 1, December 2017, Pages 20-26

Thermal Stability of Au@Pd Core/Shell Nanoparticles with Different Hollow Au Cores: Molecular Dynamics Study

S. SENTURK DALGIC

Trakya University, Department of Physics, 22030, Edirne, Turkey

Abstract:
The thermal behaviors of the core/shell spherical Au@Pd nanoparticles (NPs) with different hollow Au core sizes for the diameter of 7 nm and 8 nm NPs were first investigated by molecular dynamics (MD) simulations. Size effect on their thermodynamic stability related to the melting behavior was examined by caloric curves, the specific heat capacity, self-diffusion coefficients and total radial distribution functions under continuous heating process. The predicted results for four hollow NPs were evaluated by comparing with those obtained for the solid core-shell $Au_{0.42}@Pd_{0.58}$ and $Au_{0.63}@Pd_{0.37}$ NPs. The hollow Au@Pd NPs with thin Pd shells exhibited less thermodynamic stability and smaller melting point than those of the solid ones with the same size. A two stage melting process was observed clearly for only one hollow NPs within the Pd rich compositions. The negative heat capacity occurs only at the second stage melting in hollow core-shell of $Au_{0.34}@Pd_{0.66}$ NPs. These results indicate that the composition of hollow Au@Pd NPs together with hollow size is more important than the shell thickness of NPs. Thus, an atomistic insight into the size and thermal effect on the hollow NPs has presented for the future construction of core-shell type Au@Pd nano catalysts with hollow structures.
Keywords: Au@Pd - Core-shell Nanoparticles - Hollow Structures - Thermal Effect - Simulation.
DOI:

1. Introduction

In recent years, Bimetallic nanoparticles (NPs) containing two different elements have received considerable attention as they allow the development and design of novel structures with individual characteristics not observed in monometallic and bulk materials [1,2]. Also, among bimetallic NPs, particularly ones with core-shell (CS) structure have attracted more interest from researchers over the past few decades due to superior properties [3-16]. The CS structures are represented as @ sign to separate the shell and core structures. The different types of architectures are suitable for producing the CS structures, including single shell, multiple shells, a continuous porous shell and core, hollow core [4]. Among the different classes of CS structures, concentric spherical structures are the most common where an inner core surrounded by one or multi-shell of different material. From another point of view, there is a wide range of different combinations for choosing the core and shell material such as inorganic/inorganic, inorganic/organic, organic/inorganic and organic/organic. According to the purposes, they have extensively studied in different fields of applications such as electronics, optics sensors and catalysis [4-16].

On this line, among the developed CS structures, bimetallic nanocatalysts which is an essential class in catalysis. Thermal stability of bimetallic nanocatalysts is of the considerable importance of their applications. It is known that catalytic reactions occur on surfaces. For this reason, surface structures of nanocatalysts play key roles during the catalytic process. The performances of catalysts thereby strongly depend on their surface structures [17]. The researchers have noted that for face centered cubic (fcc) metals such as Au, Ag, Pd, Pt, etc., among all crystallographic planes that terminate the nanocrystal surface, high index facets demonstrate excellent activity and selectivity for chemical reactions compared with low index facets. However, high index facets disappear easily during the nanoparticle experiments because the rate of crystal growth in the direction perpendicular to a high index facet with high surface energy is much faster than that along the normal direction of a low-index one [17]. Therefore, increasing efforts have

Corresponding Author E-mail: dserap@*yahoo.com*

been devoted to the high index faceted bimetallic CS-NPs because they may expect to exhibit high catalytic activity compared to the monometallic ones [17-20]. Especially, the CS structure of Au@Pd was chosen to be investigated by atomistic simulations because of the experimental evidence of the best electrocatalytic activity in Au-Pd CS nanocatalysts with Tetrahexahedral, Concave Octahedral, and Octahedral Structures [17-20]. However, it has been noted in those studies that the excellent chemical activities of bimetallic NPs are highly dependent on both the surface structures of the particles and their component distribution [17].

More recently, another strategy about the surface structures has been followed to prepare bimetallic NPs with hollow interiors [13-16, 21-23]. At that point, hollow structures in comparison among metal NPs, with the same size show more catalytic activity due to their outer and inner surfaces can interact with reactants. In fundamental researches, Dalgic has investigated the thermal stability of hollow gold nanoparticles (HGNPs) with shell-core-shell structured using both bond-order-length-strength (BOLS) correlation model and MD simulations [21]. HGNPs was shown more active surfaces and surface energies than solid ones. Huang has also reported the diverse melting modes and structural collapse of hollow bimetallic CS NPs for Au@Pt and Pt@Au by MD simulations [22]. A new molecular insight into the thermodynamic evolution of hollow bimetallic CS NPs has presented by two stage melting phenomena which was first observed in hollow Au@Pt CS nanoparticle, remarkably different from the solid one.

In experiments with hollow structures of Au@Pd, Hsu and co-workers have investigated the electrochemical activities of hollow Au Core Au@Pd NPs with 10 nm Pd thick shell and diameter of 100 nm sizes [14,15]. They have reported that hollow Au@Pd CS NPs show superior catalytic activities for FAO, stability, CO oxidation ability, and long-term durability than the Pd black. More, hollow Au-Pd CS NPs show the highest current density for the ethanol oxidation reactions (EOR) in alkaline medium. It may note that modulating and controlling of these parameters are also depended on the method used for the synthesis of the nano-particles**.** However, another significant phenomenon is possible to observe that the hollow nanostructures similar to nanovoids and nanocavities may become shrinkage or collapse at elevated temperatures which are strongly affected their physical and chemical properties [21]. The hollow NPs are complex structures apparently obtained in experiments. Therefore, theoretical studies could help to understand the thermal stability behaviors of hollow nanoparticles (HNPs). MD simulations are also a powerful tool to correlate the geometric parameters with the material stability instead of the direct material synthesis. Despite the theoretically predicted thermal stability of different shape of Au@Pd and Pd@Ag CS NPs, a detailed knowledge of the thermodynamic behaviors of hollow Au@Pd CS particles is still lacking. According to our knowledge, there is not any theoretical investigation based on an atomic insight into the underlying mechanism to explain the thermal stability of hollow Au@Pd in geometrically CS structure. The primary aim of this work is to present a computational model for the thermal stability of hollow Au@Pd CS-NPs with sub diameters of 10nm which can be easily implemented in MD simulations.

2. Materials and Method

Model Construction:

The simulated solid and hollow Au@Pd core-shell NPs were constructed through a top-down method. In this study, two NPs with spherical morphology and a total number of atoms N= 10606 and N=15972 were created as a core-shell structure with 0.5 nm and 1 nm shell thickness of Pd. The corresponding compositions of Au and Pd atoms in the Au@Pd core-shell structure are given in Table 1.

Table 1. Size of the Au@Pd core-shell solid and hollow NPs used in MD simulations.

	Solid Au@Pd Core-shell NPs		Hollow Au@Pd core-shell NPs			
Size of NPs	Composition of $Au_x@Pd_y$	Total Number of atoms	Composition of hollow Au_xPd_y	Number of atoms	Radius of hollow (nm)	Pd Shell thickness (nm)
7nm	$Au_{0.63}Pd_{0.37}$	10606	$Au_{0.62}Pd_{0.38}$	10370	1nm	0.5nm
			$Au_{0.55}Pd_{0.45}$	8680	2nm	
8nm	$Au_{0.58}Pd_{0.42}$	15972	$Au_{0.34}Pd_{0.66}$	15736	1nm	1nm
			$Au_{0.41}Pd_{0.59}$	14046	2nm	

By cutting in the [111] crystallographic direction using a series of spherical cut off centered at a core of Au@Pd sphere and then, removing atoms from the center of the nanoparticle leaves a cavity space inside and thus forms a hollow Au core-shell nanoparticle. The four different size of Au@Pd core-shell NPs are formed as one-three-layer shell contains Pd atoms with different atomic ratios of Au. The compositions and number of atoms studied here are given in Table 1 where the composition of each constituent has calculated as $x=N_{Au}/N_{tot}$, $y=N_{Pd}/N_{tot}$ where N_{Au} and N_{Pd} are the numbers of atoms of Au

Corresponding Author E-mail: dserap@*yahoo.com*

and Pd elements, respectively in each nanoparticle. DLPOLY classic simulation code establishes in our MD simulations [24].

Interatomic Potentials:

In our MD calculations, the quantum corrected Sutton-Chen (Q-SC) type potentials [25,26] were adopted to describe the interatomic interactions in core-shell hollow Au@Pd NPs with different sizes. The total energy of the system is given by

$$U_{tot} = \sum_i U_i = \sum_i \varepsilon \left[\sum_{j \neq i} \frac{1}{2} V(r_{ij}) - c\rho_i^{1/2} \right] \quad (1)$$

Here, c is dimensionless parameter, and $V(r_{ij})$ is a pair potential between atoms i and j given by

$$V(r_{ij}) = \left(\frac{a}{r_{ij}} \right)^n \quad (2)$$

The local electron density contribution of atom i is written as

$$\rho_i = \sum_{j \neq i} \varphi(r_{ij}) = \sum_{j \neq i} \left(\frac{a}{r_{ij}} \right)^m \quad (3)$$

Those potential parameters have optimized according to the lattice parameter, cohesive energy and bulk modulus of pure gold and Pd. Possible parameters used in atomistic simulations can be found elsewhere [17, 26]. Q-SC parameters include quantum corrections and take the zero-point energy.

Simulation Procedure:

The nanoparticles are simulated with constant temperature and constant volume (NVT) molecular dynamics without the periodic boundary conditions. Brendsden thermostat was applied in NVT–MD simulations with 0.5 values. The leapfrog Verlet velocity algorithm was integrated with the equations of atomic motions. The time step of simulations is 0.025 ps. The MD simulations have been carried out 300000 steps, and during atomic coordinates, velocities and energies were extracted for the statistical quantities in the last 200000 steps. All the nanoparticles became the stable state after enough steps to reach the potential plateau.

3. Results and Discussion

Here, MD simulations were established by the core-shell Au@Pd NPs given in Table 1. The atomic arrangements of 8 nm size Au@Pd core-shell NPs without and with hollow interior are shown in Figure1.a - Figure 1.b, respectively. The snapshots of cross sections perspective view and sliced in [010] direction of the CS Au@Pd NPs for the atomic arrangements of the 4 nm radius with N15972 atoms are illustrated in Figure 2.a and with the 2 nm thickness of Au core Figure 2.b, respectively. OVITO package is used to demonstrate these atomic arrangements [27].

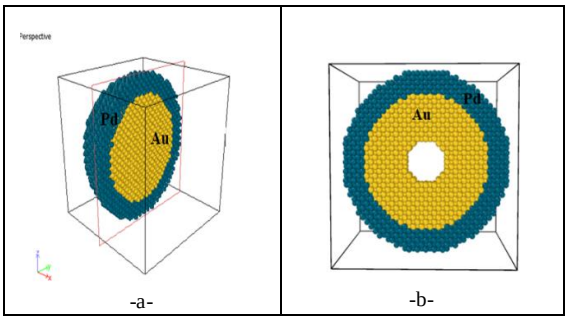

Figure 1. Snapshoots of the atomic arrangements of 8 nm size (a) Au@Pd core-shell and (b) with the 1 nm radius of the hollow interior of Au@Pd core- shell NPs at 300 K. Coloring denotes the type of atom: yellow, Au atom; dark green Pd atom.

Au@Pd Core-shell NPs:

In this study, first Au@Pd core-shell NPs composed of Au core with Pd shell were simulated. The temperature dependence of cohesive energy has been shown in Figure 2 for the 3 nm radius of Au core with a different shell thickness of Au@Pd nanoparticle. The isochoric specific heat capacities (C_v) per atom for the corresponding energies are also given in the same figure as a function of temperature. As seen in Figure 2, the cohesive energy increases linearly with temperature, whereas an abrupt change is observed at high temperatures for each NPs. In order to identify the temperature of first order phase transition as a solid-liquid phase transition, the variation of the total energy and the specific heat capacity at constant volume was computed for the NPs. Thus the melting temperature can define as the temperature corresponds to the maximum peak value in the heat capacity which is in good agreement with a simple jump of the energy in the caloric curve.

Corresponding Author E-mail: dserap@*yahoo.com*

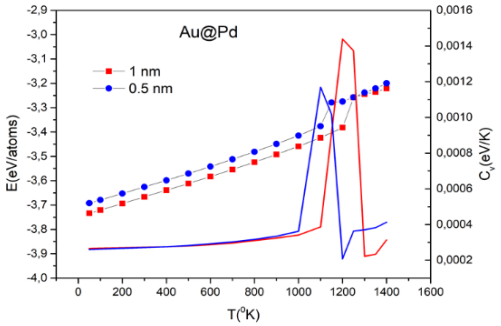

Figure 2. Temperature dependence of cohesive energies and the corresponding isochoric heat capacities per atom for the 4 nm radius of Au@Pd NPs with variable shell thickness.

Notably, as seen in Figure 2, cohesive energy decreases when the size reduced. This trend is observed in MD simulations of 7 nm size Au@Pd NPs; one can see that larger NPs have lower energies and higher melting points and thermodynamic stability. However, two-step melting mode is not observed for Au@Pd core-shell NPs. The melting point of the Au@Pd core-shell NPs are obtained as 1150 K and 1210 K for the shell thickness of Pd with 0.5 nm and 1 nm, respectively. These results agree with other similar calculations [17-20].

Hollow Au@Pd Core-shell NPs:

In this study, the thermodynamic stability of hollow Au@Pd NPs at different temperatures have investigated through the changes in morphology and the thermodynamic properties during the heating process, such as snapshots of atomic arrangements at different temperatures, caloric curves, heat capacity and self-diffusion coefficients. In order to investigate the thermal behavior of the simulated hollow Au@Pd core-shell NPs, detailed in Table 1, snapshots from their cross sections in [010] direction are illustrated in Figure 3. For the NPs with variable shells include 1 nm and 2 nm hollow interior in Figure 3.a and Figure 3.b, respectively, the collapsing mechanism has just occurred in thin shell nanoparticle at the temperature of 1050 K. Therefore, Figure 3 is also presented size dependent first stage melting of hollow Au@Pd CS NPs.

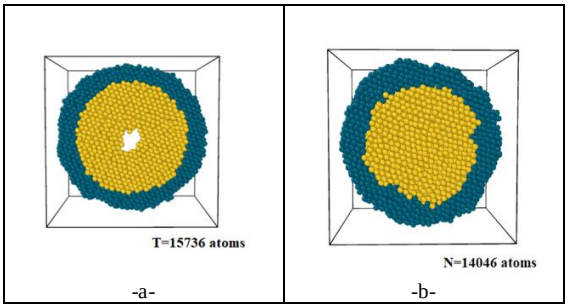

Figure 3. Snapshots of cross sections for the different hollow size of Au@Pd NPs with (a) N=15736 atoms and (b) 14046 atoms at the same temperature of 1050 K.

At the first stage, melting starts from the inner surface. Than, CS nanoparticle becomes a liquid core-solid shell structure and finally transforms into a mixing alloy (second stage melting). It can be seen that it has definitely occurred for the hollow Au@Pd nanoparticle with N=14046 and partially observed for the hollow one with N=15736. The caloric curves and corresponding specific heat capacities for hollow Au@Pd NPs are shown in Figure 4.

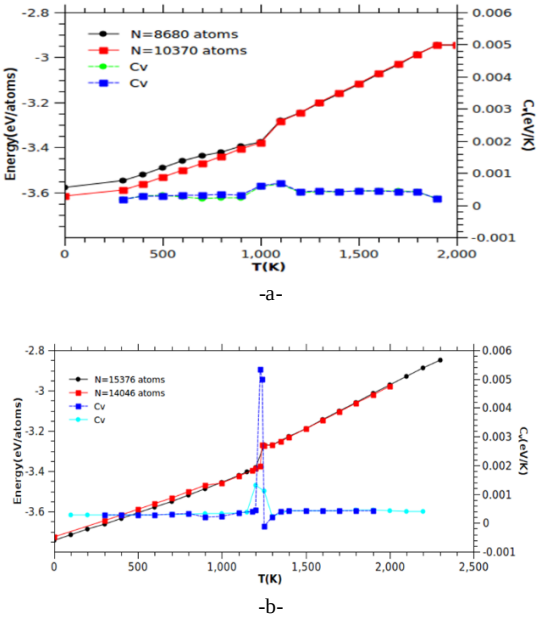

Figure 4. Caloric curves and the corresponding isochoric heat capacities per atom for (a) 3,5 nm and (b) 4 nm radius of hollow Au@Pd NPs with variable Pd shell thickness.

As can be seen from Figure 3, the NPs with smaller core sizes are more stable because of the difference of Au and Pd energies. However, for other hollow Au@Pd CS nanoparticles, the overall melting occurs during the collapse of the hollow structure because of more Au atoms than Pd atoms. The bulk melting point of Au is 1337 K which is close to the bulk melting of Pd. As can be observed in Figure 4, the melting temperature is defined by the sharp rise of.

Corresponding Author E-mail: dserap@*yahoo.com*

cohesive energy and the abrupt peak of the heat capacity. Because of the second stage melting, the negative heat capacity has been observed in hollow $Au_{0.34}@Pd_{0.66}$ NPs with N=14046 atoms. In Figure 4, the cohesive energy exhibits different degrees of decrease beyond phase transition. Larger core size (for $Au_{0.34}@Pd_{0.66}$) leads to more reduction as seen in Figure 4. It is associated with the atomic diffusion of atoms after overall melting as shown in Figure 5. The self-diffusion behaviors of atoms are illustrated in Figure 5 for different composition of hollow CS NPs.

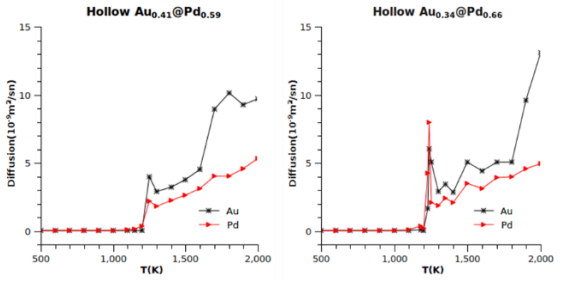

-a- -b-

Figure 5. Self-diffusion coefficients of Au and Pd atoms in hollow core-shell NPs of (a) $Au_{0.41}@Pd_{0.59}$ with N=15736 atoms and (b) $Au_{0.34}@Pd_{0.66}$ with N=14046 atoms.

For the thermal evolution under the continues heating process, the diffusivity of atoms is also an essential issue because of its technologic importance for application in catalysts. As is obvious from Figure 5 that the diffusivity shows a rapid increase in the evaluated temperature. This is related to the component redistribution in bimetallic CS NPs. Therefore, the total/pair radial distribution function of the NPs at different temperatures is of importance to explore the catalytic properties of NPs. Figure 6 shows the total radial distribution function (RDF) of hollow CS $Au_{0.34}@Pd_{0.66}$.

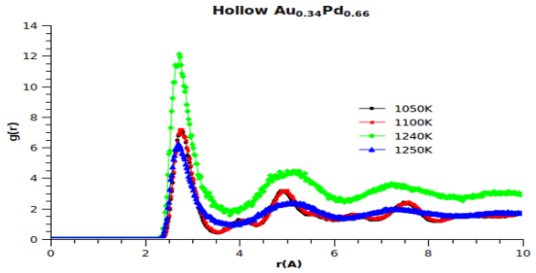

Figure 6. Total radial distribution functions of hollow CS NP of $Au_{0.34}@Pd_{0.66}$ with N=14046 atoms at different temperatures.

Figure 6 is agreeing with the results presented in Figures 3-5. It can be seen from Figure 6 that after collapsed hollow part at 1050 K, the amorphous phase can be observed. The second stage melting occurs at 1250 K; the g(r) function behaves like a liquid. By analyzing the atomic distribution function, the separation or aggregation behavior of NPs induced by the diffusion can be defined.

4. Conclusion

In this work, MD simulations were employed with Q-SC model potentials to investigate the thermal stability of Au@Pd NPs with hollow structures. The caloric curves, morphologic changes, heat capacity, self-diffusions and g(r) total distribution function under heating process were computed to examine the thermal stability of these NPs. The size-dependent cohesive energies of hollow Au@Pd CS NPs are presented. A typical two stage melting is exhibited only for the Pd rich composition of hollow CS NPs for $Au_{0.34}@Pd_{0.66}$. The predicted results are also agreeing with Huang's calculations and provide a fundamental perspective for hollow CS Au@Pd NPs with a diameter of 7-8 nm (sub<10 nm). The critical temperature of first stage melting of $Au_{0.41}@Pd_{0.59}$ (N=15736) is lower than that of $Au_{0.34}@Pd_{0.66}$ NPs (N=14046) because of the existence of stacking faults at low temperatures. Atomic structures of these NPs will be presented in the near future by comparing the intermetallic hollow Pd3Au NPs.

References

[1] H. Liao, A. Fisher, and J. Xu, Zhichuan," Bimetallic Nanoparticles: Surface Segregation in Bimetallic Nanoparticles: A Critical Issue in Electrocatalyst Engineering (Small 27/2015)" 11, 3221, 2015.
Doi: 10.1002/smll.201403380

[2] S. Alayoglu, F. Tao, V. Altoe, C. Specht, Z. Zhu, F. Aksoy, D. Butcher, R. Renzas, Z.Liu, G. Somorjai, " Surface Composition and Catalytic Evolution of AuxPd1−x (x = 0.25, 0.50 and 0.75) Nanoparticles Under CO/O2 Reaction in Torr Pressure Regime and at 200 °C" Catal. Lett. 141, 633, 2011.
Doi:10.1007/s10562-011-0565-7

[3] D. Wang, Y. Li, "Bimetallic Nanocrystals: Bimetallic Nanocrystals: Liquid-Phase Synthesis and Catalytic Applications, Adv. Mater., 23, 1044, 2011.
Doi:10.1002/adma.201003695

[4] R. Ghosh Chaudhuri, S. Paria, "Core/Shell Nanoparticles: Classes, Properties, Synthesis Mechanisms, Characterization, and Applications "Chem. Rev., 112, 2373, 2012.

Corresponding Author E-mail: dserap@*yahoo.com*

Doi: 10.1021/cr100449n

[5] R. Ferrando, J. Jellinek and R. L Johnston, "Nanoalloys: From Theory to Applications of Alloy Clusters and Nanoparticles" Chem. Rev. 108, 845, 2008.
Doi: 10.1021/cr040090g.

[6] S.J. Oldenburg, R.D. Averitt, S.L. Westcott, N.J. Halas, " Nanoengineering of optical resonances" Chem. Phys. Lett., 288, 243, 1998.

[7] L. Feng, G. Gao, P. Huang, K. Wang, X. Wang, T. Luo, C. Zhang, „ Optical properties and catalytic activity of Bimetallic Gold-Silver Nanoparticles" Nano Biomed. Eng., 2, 258, 2010.
Doi: 10.5101/nbe.v2i4

[8] W.-Y. Yu, G. M. Mullen, D. W. Flaherty and C.B. Mullins, "Selective Hydrogen Production from Formic Acid Decomposition on Pd-Au Bimetallic Surfaces" J. Am. Chem. Soc.,136, 11070, 2014.
Doi: 10.1021/ja505192v

[9] A Samanta, T Rajesh, R. N Devi, " Confined space synthesis of fully alloyed and sinter resistant AuPd nanoparticles encapsulated in porous silica" J. Mater. Chem. A, 2, 4398, 2014.
Doi: 10.1039/C3TA15194H

[10] G. Yang, D. Chen, P. Lv, X. Kong, Y. Sun, Z. Wang, Z. Yuan, H. Liu and J. Yang, " Core-shell Au-Pd nanoparticles as cathode catalysts for microbial fuel cell applications" Sci. Rep. 6, 35252, 2016.
Doi: 10.1038/srep35252

[11] C. Li, Y. Su, X. Lv, Y. Zuo, X. Yang, Y. Wang, "Au@Pd core–shell nanoparticles: A highly active electrocatalyst for amperometric gaseous ethanol sensors" Sensors and Actuators B, 171-172, 1192, 2012.
Doi: 10.1016/j.snb.2012.06.073

[12] Q. Tan, C. Du, G. Yin, P. Zuo, X. Cheng, M. Chen, " Highly efficient and stable nonplatinum anode catalyst with Au@Pd core–shell nanostructures for methanol electrooxidation" J. Catalysis, 295, 217, 2012.
Doi: 10.1016/j.jcat.2012.08.016.

[13] C. Hsu, C. Huang, Y. Hao and F. Liu, Int. J. "Electro-oxidation of formate-based solutions on Au/Pd core–shell nanoparticles – Experiment and simulation" Hydrogen Energy, 38, 15532, 2013.
Doi: 10.1016/j.ijhydene.2013.09.019

[14] C. Hsu, C. Huang, Y. Hao and F. Liu, Int. " Impact of surface roughness of Au core in Au/Pd core–shell nanoparticles toward formic acid oxidation – Experiment and simulation" J. Power Sources, 243, 343, 2013.
Doi: 10.1016/j.jpowsour.2013.05.185

[15] C. Hsu, C. Huang, Y. Hao, F. Liu, " Au/Pd core-shell nanoparticles with varied hollow Au cores for enhanced formic acid oxidation" Nanoscale Res. Lett. 8, 113, 2013.
Doi: 10.1186/1556-276X-8-113

[16] H. M. Song, D. H. Anjum, R. Sougrat, M. N. Hedhili and N. M. Khashab, " Hollow Au@Pd and Au@Pt core–shell nanoparticles as electrocatalysts for ethanol oxidation reactions " J. Mater. Chem., 22, 25003, 2012.
Doi: 10.1039/c2jm35281h

[17] R. Huang, Y-H Wen, G.-F Shao, Z-Z Zhu and S.-G. Sun, "Thermal Stability and Shape Evolution of Tetrahexahedral Au–Pd Core–Shell Nanoparticles with High-Index Facets" J. Phys. Chem. C, 117, 6896, 2013.
Doi: 10.1021/jp401423z

[18] A. Spitale, M. A. Perez, S. Mejía-Rosales, M. J. Yacaman, and M. M. Mariscal, "Gold-Palladium core@shell nanoalloys: experiments and simulations" Phys Chem Chem Phys, 17, 28060, 2015.
Doi: 10.1039/c4cp06012a.

[19] G-F.Shao, N-N.Tu, T.-D. Liu, L.-Y. Xu and Y.-H. Wen, Physica E, 70, 11, 2015.
Doi: 10.1016/j.physe.2015.02.008

[20] C. Fernandez-Navarro and S. Mejía-Rosales, " Stability of Au- Pd Core-Shell Nanoparticles" J. Phys. Chem. C,121, 21658, 2017.
Doi: 10.1021/acs.jpcc.7b04564

[21] S. Senturk Dalgic, "Size Dependent Properties of Hollow Gold Nanoparticles: A Theoretical Investigation" Acta Physica Polonica A, 294, 531, 2016.
Doi: 10.12693/APhysPolA.129.531

[22] R. Huang, G.-F. Shao, X-M. Zeng and Y-H. Wen, "Diverse Melting Modes and Structural Collapse of Hollow Bimetallic Core-Shell

Corresponding Author E-mail: dserap@*yahoo.com*

Nanoparticles: A Perspective from Molecular Dynamics Simulations" Sci. Rep. 4, 7051, 2014. Doi:10.1038/srep07051

[23] H. Akbarzadeh, E. Mehrjouei, A. N. Shamkhali, M. Abbaspour, S. Salemi and S. Ramezanzadeh, "New Molecular Insight into the Stability of Ni-Pd Hollow Nanoparticles" Inorg. Chem. Front., 4, 1679, 2017. Doi: 10.1039/C7QI00370F

[24] DL_POLY: a molecular dynamics simulation package was written by W. Smith, T.R. Forester, and I.T. Todorov obtained from the website http://www.ccp5.ac.uk/DL_POLY

[25] A. Sutton, J. Chen, "Long-Range Finnis Sinclair Potentials" Philos. Mag. Lett., 61, 139, 1990. Doi: 10.1080/09500839008206493

[26] T. Cagin, Y. Kimura, Y. Qi, H. Li, H. Ikeda, W. L. Johnson, W.A. Goddard, " Calculation of Mechanical, Thermodynamic and Transport Properties of Metallic Glass Formers" Mater. Res. Soc. Symp. Proc. 554, 43, 1999. Doi: 10.1557/PROC-554-43

[27] A. Stukowski, "Visualization and analysis of atomistic simulation data with OVITO–the Open Visualization Tool" Modelling Simul. Mater. Sci. Eng. 18, 015012, 2010. Doi: 10.1088/0965-0393/18/1/015012

Corresponding Author E-mail: dserap@*yahoo.com*